Linearized Pair-Density Functional Theory

Matthew R. Hennefarth,[†] Matthew R. Hermes,[†] Donald G. Truhlar,[*,‡] and Laura Gagliardi[*,¶]

[†]*Department of Chemistry, Pritzker School of Molecular Engineering, The James Franck Institute, and Chicago Center for Theoretical Chemistry, University of Chicago, Chicago, IL 60637, USA*

[‡]*Department of Chemistry, Chemical Theory Center, and Minnesota Supercomputing Institute, University of Minnesota, Minneapolis, MN 55455-0431, USA*

[¶]*Argonne National Laboratory, 9700 S. Cass Avenue, Lemont, IL 60439, USA*

E-mail: *truhlar@umn.edu; *lgagliardi@uchicago.edu

Abstract

Multiconfiguration pair-density functional theory (MC-PDFT) is a post-SCF multireference method that has been successful at computing ground- and excited-state energies. However, MC-PDFT is a single-state method in which the final MC-PDFT energies do not come from diagonalization of a model-space Hamiltonian matrix, and this can lead to inaccurate topologies of potential energy surfaces near locally avoided crossings and conical intersections. Therefore, in order to perform physically correct *ab initio* molecular dynamics with electronically excited states or to treat Jahn-Teller instabilities, it is necessary to develop a PDFT method that recovers the correct topology throughout the entire nuclear configuration space. Here we construct an effective Hamiltonian operator, called the linearized PDFT (L-PDFT) Hamiltonian, by expanding the MC-PDFT energy expression to first order in a Taylor series of the wave function density. Diagonalization of the L-PDFT Hamiltonian gives the correct potential energy

surface topology near conical intersections and locally avoided crossings for a variety of challenging cases including phenol, methylamine, and the spiro cation. Furthermore, L-PDFT outperforms MC-PDFT and previous multi-state PDFT methods for predicting vertical excitations from a variety of representative organic chromophores.

1 Introduction

Understanding and properly modeling excited-state dynamics is important for many photo-induced processes in chemistry and biochemistry including photochemistry,[1,2] light-harvesting,[3–5] photocatalysis,[6–8] photosensing,[9] vision,[10,11] DNA photostability,[12] and nonadiabatic electron transfer.[13] Multiconfiguration pair-density functional theory[14] (MC-PDFT) is a post-SCF method that that has been shown to be a computationally efficient method for computing potential energy surfaces (PESs) of excited states.[15,16] Starting from a multiconfigurational wave function, such as that provided by the complete active space SCF (CASSCF) method, MC-PDFT computes a corrected energy through a nonvariational energy expression which is a functional of the electron density (ρ) and on-top pair density (Π). Consequently, the MC-PDFT energies are not eigenvalues of any particular Hamiltonian or quantum operator, and the energy of each state is computed independently of the other states involved in the calculation. MC-PDFT and its hybrid counterpart (HMC-PDFT)[17] have been shown to perform similarly to the much more expensive n-electron valence perturbation theory (NEVPT2)[18] for over 300 vertical excitations in the QUESTDB database.[16]

When modeling photochemistry and photodynamics, one frequently encounters locally avoided crossings and conical intersections: regions in which states of the same spin symmetry interact strongly with each other. This necessitates the use of an electronic structure method that includes state interaction to prevent unphysical PES crossings near these strong coupling geometries. Such methods are called multi-state methods,[19] and they include multi-state[20,21] and quasi-degenerate[22–24] perturbation theory as well as multireference configuration interaction.[19,25] They are necessary for a proper treatment of nonadiabatic dynamics or

Jahn-Teller instabilities.

The original MC-PDFT method is a single-state method, but recent research has provided multi-state extensions. State-interaction PDFT[26] was the first such extension, and involved two sets of orbitals for the ground and excited states. Later, methods involving only a single set of state-averaged CASSCF (SA-CASSCF) orbitals were constructed and these are called multi-state PDFT (MS-PDFT).[27,28] The MS-PDFT methods diagonalize an effective model space Hamiltonian matrix in an intermediate basis where the off-diagonal elements come from the underlying wave function theory, and the diagonal elements are replaced with the MC-PDFT energies of the intermediate states. The various MS-PDFT methods differ only in the choice of intermediate states, and the results are sometimes sensitive to this choice.

Of the various MS-PDFT methods, compressed multi-state PDFT (CMS-PDFT) has been shown to have the best balance of computational efficiency and accuracy for the widest variety of systems, and it computes PESs similar to the more expensive extended multi-state complete-active-space 2nd-order perturbation theory (XMS-CASPT2) for a variety of test cases.[28] However, during the development of CMS-PDFT analytical gradients,[29] it was discovered that CMS-PDFT struggles with linear molecules with degenerate $^1\Delta_u$ states. For these structures, the CMS-PDFT energies are non-unique, and the CMS-PDFT PESs can be discontinuous. A second disadvantage of CMS-PDFT is that the intermediate-state basis is obtained by solving a nonlinear system of equations, and there is no guarantee that this solution is uniquely defined for a given molecular geometry, atomic-orbital basis, active space, and model space. This additional non-convex global optimization step thus carries additional risk of not converging the iterations or converging to inequivalent local minima of the intermediate-state objective function. It is desirable to have a MS-PDFT method that yields a unique energy for any nuclear configuration, does not have an iterative procedure to find intermediate states, is able to handle a wide variety of systems, and preserves both spatial and spin symmetries. That is the goal of the work presented here.

In this paper, we introduce a new multi-state PDFT method called linearized PDFT

(L-PDFT) in which we express the Hamiltonian ($\hat{H}^{\mathrm{L-PDFT}}$) in second quantization as an operator that is a functional of the density and pair density. We construct $\hat{H}^{\mathrm{L-PDFT}}$ by expanding the MC-PDFT energy functional in a power series of ρ and Π variables about their state-averaged values within the model space and truncate this series at first order, such that for any state $|I\rangle$, $\langle I|\hat{H}^{\mathrm{L-PDFT}}|I\rangle$ is a linear approximation to its MC-PDFT energy. By construction, $\hat{H}^{\mathrm{L-PDFT}}$ is a well-defined linear operator whose off-diagonal elements are generally nonzero, and diagonalization of $\hat{H}^{\mathrm{L-PDFT}}$ within a given subspace yields a set of PES with the correct topology near conical intersections and locally avoided crossings. Here we show that L-PDFT yields similar PES topology to CMS-PDFT for a variety of challenging cases including phenol, methylamine, and the spiro cation and, it does not have the same intrinsic limitations of CMS-PDFT for linear systems with degenerate $^1\Delta_u$ states (see Section 4.6). Additionally, we compute the vertical excitation energy for a small test set of representative organic chromophores and find that L-PDFT is more accurate than MC-PDFT and CMS-PDFT.

2 Theory

2.1 Notation

Capital letters I, J label general many-electron states. Lowercase letters p, q, r, s, t, u label general spatial molecular orbitals. Repeated indices are summed implicitly. Boldfaced characters represent tensors (vectors, matrices, etc.).

2.2 Multiconfiguration Pair-Density Functional Theory (MC-PDFT)

MC-PDFT is a post-SCF method that computes the energy of a state using a functional expression similar to Kohn-Sham density functional theory (KS-DFT). The MC-PDFT energy

expression for some state $|I\rangle$ is defined as

$$E_I^{\mathrm{MC-PDFT}} = h_{\mathrm{nuc}} + h_{pq}D_{pq}^I + \frac{1}{2}g_{pqrs}D_{pq}^I D_{rs}^I + E_{\mathrm{ot}}[\rho_I, \Pi_I] \tag{1}$$

where h_{nuc} is the nuclear-nuclear repulsion term, h_{pq} and g_{pqrs} are the 1- and 2-electron integrals, D_{pq}^I and d_{pqrs}^I are elements of the spinless reduced 1- and 2-particle density matrices of state $|I\rangle$ ($\mathbf{D}^I$ and $\mathbf{d}^I$ respectively), and E_{ot} is an on-top density functional of the density, ρ_I, and on-top density, Π_I.[14] Summing all terms except the on-top functional equals the sum of the kinetic energy and classical electrostatic energy for the state.

Given a set of spatial molecular orbitals, $\phi_p(\mathbf{r})$, both ρ_I and Π_I can be expressed as functions of $\mathbf{D}^I$ and $\mathbf{d}^I$:

$$\rho_I(\mathbf{r}) = D_{pq}^I \phi_p^*(\mathbf{r})\phi_q(\mathbf{r}) \tag{2a}$$

$$\Pi_I(\mathbf{r}) = \frac{1}{2}d_{pqrs}^I \phi_p^*(\mathbf{r})\phi_q(\mathbf{r})\phi_r^*(\mathbf{r})\phi_s(\mathbf{r}) \tag{2b}$$

Thus, the MC-PDFT energy expression (Eq. 1) can be expressed as an explicit function of the 1- and 2-particle density matrices for a given state:

$$E_I^{\mathrm{MC-PDFT}}\left(\mathbf{D}^I, \mathbf{d}^I\right) = h_{\mathrm{nuc}} + h_{pq}D_{pq}^I + \frac{1}{2}g_{pqrs}D_{pq}^I D_{rs}^I + E_{\mathrm{ot}}\left[\mathbf{D}^I, \mathbf{d}^I\right] \tag{3}$$

2.3 Linearized-PDFT (L-PDFT)

The classical electrostatic and on-top functional terms in Eq. 1 are nonlinear in the densities. The Coulomb term is quadratic with respect to $\mathbf{D}^I$, and in general, the on-top functional is even more nonlinear in the densities. This means that it is generally not possible to find an operator $\hat{O}$ such that

$$E_I^{\mathrm{MC-PDFT}} = \langle I|\hat{O}|I\rangle \tag{4}$$

for every state $|I\rangle$. Instead, we can linearly approximate the MC-PDFT energy expression to find a linearized PDFT (L-PDFT) Hamiltonian $\hat{H}^{\mathrm{L-PDFT}}$ such that for any state $|I\rangle$

$$E_I^{\mathrm{MC-PDFT}} \approx \langle I|\hat{H}^{\mathrm{L-PDFT}}|I\rangle \tag{5}$$

We proceed by Taylor expanding both the classical Coulomb and on-top functional terms in a power series of $\mathbf{D}^I$ and $\mathbf{d}^I$ around some zeroth-order densities ($\mathbf{D}^0$ and $\mathbf{d}^0$) and truncate after first order. We truncate after first order because we want a linear function of the densities $\mathbf{D}, \mathbf{d}$. If we go to second order, we will recover the exact classical Coulomb term as already present in the MC-PDFT energy expression (Eq. 1), but we will not be able to extract an effective Hamiltonian operator. Since the Coulomb term only depends on $\mathbf{D}^I$, to first order we obtain

$$\frac{1}{2}g_{pqrs}D^I_{pq}D^I_{rs} \approx \frac{1}{2}g_{pqrs}D^0_{pq}D^0_{rs} + \frac{1}{2}g_{pqrs}\left(\delta_{pq,tu}D^0_{rs} + \delta_{rs,tu}D^0_{pq}\right)\left(D^I_{tu} - D^0_{tu}\right) \tag{6}$$

Here, $\delta_{pq,rs}$ is the standard Kronecker delta. Simplification and using the permutation symmetry of the 2-electron integrals allows us to write the Coulomb term as

$$\frac{1}{2}g_{pqrs}D^I_{pq}D^I_{rs} \approx \mathcal{J}^0_{pq}D^I_{pq} - \frac{1}{2}g_{pqrs}D^0_{pq}D^0_{rs} \tag{7}$$

where

$$\mathcal{J}^0_{pq} = g_{pqrs}D^0_{rs} \tag{8}$$

is the Coulomb interaction with the zeroth-order density. Expanding the on-top functional term to first order allows us to write

$$E_{\mathrm{ot}}[\mathbf{D}^I, \mathbf{d}^I] \approx E_{\mathrm{ot}}[\mathbf{D}^0, \mathbf{d}^0] + \left(\mathbf{D}^I - \mathbf{D}^0\right)\cdot\nabla_{\mathbf{D}}E_{\mathrm{ot}}[\mathbf{D}^0, \mathbf{d}^0] + \left(\mathbf{d}^I - \mathbf{d}^0\right)\cdot\nabla_{\mathbf{d}}E_{\mathrm{ot}}[\mathbf{D}^0, \mathbf{d}^0] \tag{9}$$

Note that both $\nabla_{\mathbf{D}} E_{\text{ot}}$ and $\nabla_{\mathbf{d}} E_{\text{ot}}$ have been defined in previous MC-PDFT analytic nuclear gradient papers[30,31] and are called the 1- and 2-electron on-top potentials, respectively, and they are given by

$$V^0_{pq} = \frac{\partial E_{\text{ot}}[\mathbf{D}^0, \mathbf{d}^0]}{\partial D_{pq}} \tag{10a}$$

$$v^0_{pqrs} = \frac{\partial E_{\text{ot}}[\mathbf{D}^0, \mathbf{d}^0]}{\partial d_{pqrs}} \tag{10b}$$

Hence, the first-order Taylor expansion of the MC-PDFT energy of state $|I\rangle$ around the zeroth-order densities $\mathbf{D}^0, \mathbf{d}^0$ is given by

$$E^{\text{MC-PDFT}}_I \approx \left(h_{pq} + \mathcal{J}^0_{pq} + V^0_{pq}\right) D^I_{pq} + v^0_{pqrs} d^I_{pqrs} + h_{\text{const}} \tag{11}$$

where we have collected all constant terms (those that do not depend on $\mathbf{D}^I$ or $\mathbf{d}^I$) as

$$h_{\text{const}} = h_{\text{nuc}} - \frac{1}{2} g_{pqrs} D^0_{pq} D^0_{rs} + E_{\text{ot}}[\mathbf{D}^0, \mathbf{d}^0] - V^0_{pq} D^0_{pq} - v^0_{pqrs} d^0_{pqrs} \tag{12}$$

Defining $\hat{H}^{\text{L-PDFT}}$ as

$$\hat{H}^{\text{L-PDFT}} = \left(h_{pq} + \mathcal{J}^0_{pq} + V^0_{pq}\right) \hat{E}_{pq} + \frac{1}{2} v^0_{pqrs} \hat{e}_{pqrs} + h_{\text{const}} \tag{13}$$

with $\hat{E}_{pq}$ and $\hat{e}_{pqrs}$ being the 1- and 2-electron excitation operators respectively, yields a quantum operator that satisfies the condition of Eq. 5.

There are several different zeroth-order densities that one can expand around. For example, one might consider expanding about the Hartree-Fock densities or the ground-state densities. However, these densities would treat the ground state on a different footing than the excited states, which is undesirable. Instead, we use the state-averaged densities given

by

$$D^0_{pq} = w_I \langle I|\hat{E}_{pq}|I\rangle \tag{14a}$$

$$d^0_{pqrs} = w_I \langle I|\hat{e}_{pqrs}|I\rangle \tag{14b}$$

where w_I satisfy

$$\sum_I w_I = 1 \tag{15}$$

and would typically be the same weights as used in a reference SA-CASSCF calculation. These densities are desirable as they will treat all the states on an equal footing.

Letting $\mathscr{U}$ be the particular subspace of the Hilbert space $\mathscr{H}$ such that $\mathscr{U}$ is the span of $\{|I\rangle\}$ (in this paper, we take $\mathscr{U}$ to be the model space which is spanned by the SA-CASSCF states, as is customary in multi-state perturbation theory and in earlier MS-PDFT methods), then for equal weights, the state-averaged densities maintain the property that they are independent of the reference state basis $\{|I\rangle\}$, making $\mathbf{D}^0$ and $\mathbf{d}^0$ functionals of the subspace $\mathscr{U}$. Hence $\hat{H}^{\mathrm{L-PDFT}}$, along with its eigenvalues and eigenvectors, are independent of the initial basis $\{|I\rangle\}$ and instead are functionals only of the subspace $\mathscr{U}$ that $\{|I\rangle\}$ span. That is, for each subspace $\mathscr{U} \subseteq \mathscr{H}$ there is a unique quantum operator $\hat{H}^{\mathrm{L-PDFT}}[\mathscr{U}]$. Whereas in KS-DFT and MC-PDFT the energy is expressed as a functional of the density of a given state, we have defined an effective Hamiltonian that is a functional of a state-averaged density within a given subspace.

Note that although the effective Hamiltonian is a functional of $\mathscr{U}$, its definition is not restricted to $\mathscr{U}$: a matrix element of Eq. (13) could be evaluated for any arbitrary pair of many-electron states in $\mathscr{H}$. However, for states outside of $\mathscr{U}$, we do not expect Eq. (5) to be adequately satisfied, since the densities of those states did not contribute to the average density which defines the operator. Therefore, in this work we project $\hat{H}^{\mathrm{L-PDFT}}[\mathscr{U}]$ into the same subspace $\mathscr{U}$ and diagonalize to yield a particular set of eigenvectors ($\{|M\rangle\}$) and eigenvalues ($\left\{E^{\mathrm{L-PDFT}}_M\right\}$). Since the $\{|M\rangle\}$ come from diagonalization of a Hermitian

operator, they should provide the correct PES topology near conical intersections and locally avoided crossings. As an anticipation of future work, we note that L-PDFT should provide simpler expressions than CMS-PDFT for analytic gradients and other response properties (such as excited-state dipole moments, transition dipole moments, and nonadiabatic coupling vectors) because the final L-PDFT states are not dependent on a nonvariationally-optimized intermediate state basis (as in CMS-PDFT).

2.4 Hybrid Linearized-PDFT

HMC-PDFT[17] extends the original Becke concept of KS-DFT hybrid functionals[32] by using a weighted average of the CASSCF and MC-PDFT energies:

$$E_I^{\mathrm{HMC-PDFT}} = \lambda E_I^{\mathrm{CAS}} + (1-\lambda) E_I^{\mathrm{MC-PDFT}} \tag{16}$$

where λ controls the fraction of CASSCF energy (E_I^{CAS}) which is included in the hybridization. We refer to hybrid calculations by using the language of hybrid functionals, for example we refer to using Eq. 16 with λ equal to 0.25 and the tPBE functional in the MC-PDFT term as an HMC-PDFT calculation with the hybrid functional tPBE0. Because it has been found that hybrid functionals, such as tPBE0, are more accurate than non-hybrid ones for certain systems,[16] we also construct a hybrid linearized PDFT (HL-PDFT) Hamiltonian. Since E_I^{CAS} is linear with respect to the densities, Taylor expanding Eq. 16 and extracting the effective HL-PDFT Hamiltonian ($\hat{H}^{\mathrm{HL-PDFT}}$) yields

$$\hat{H}^{\mathrm{HL-PDFT}} = \lambda \hat{H}^{\mathrm{el}} + (1-\lambda)\hat{H}^{\mathrm{L-PDFT}} \tag{17}$$

where $\hat{H}^{\mathrm{el}}$ is the usual electronic Hamiltonian.

3 Computational Details

We study the potential energy curves and PESs of several test systems that have been studied in prior MS-PDFT papers.[27,28] For all cases considered here except acetylene, CMS-PDFT has been shown to perform similarly to the more expensive XMS-CASPT2; hence, we use CMS-PDFT as a benchmark for those systems. For acetylene, we use XMS-CASPT2 as our benchmark because this system has not been studied previously with any MS-PDFT method. System-specific computational details including symmetry, basis set, number of states, active space electrons and orbitals, and reaction coordinates scanned are summarized in Table 1. For the spiro cation, XMS-PDFT data is taken from the supporting information of Ref 28.

Table 1: Systems for which potential curves are studied along with the symmetry, basis set, number of states (N), number of active space electrons (n_e), active space MOs used, and the internal coordinates scanned.

System	Sym	Basis Set	N	n_e	Active Space	Coordinates Scanned
LiF	C_{2v}	aug-cc-pVTZ[33,34]	2	8	2s of Li 2s, 2p of F	r(Li-F) = [1.0, 9.0] Å
LiH	C_{2v}	aug-cc-pVTZ[33,34]	4	2	2s, 2p$_z$, 3s, 3p$_z$ of Li 1s of H	r(Li-H) = [1.0, 12.0] Å
CH_3NH_2	C_1	6-31++G(d,p)[35–37]	3	6	2σ, $1\sigma^*$ 2p$_z$, 2s, 3p$_z$ of N	r(N-H) = [0.80, 3.60] Å τ(H-C-N-H) = 0°, 90°, 100°
C_6H_5OH	C_1	cc-pVDZ[33]	2	12	$3(\pi,\pi^*)$ σ_{OH}, σ^*_{OH}, σ_{CO}, σ^*_{CO} p$_z$ of O	r(O-H) = [0.65, 3.00] Å φ(C-C-O-H) = 1°, 10°
spiro[a]	C_{2v}	6-31G(d)[38]	2	11	see Ref 39	See Section 4.5
C_2H_2	C_1	aug-cc-pVDZ[33,34]	4	4	$2(\pi,\pi^*)$, $2\pi^*$	θ(C-C-H) = [135°, 179°]

[a] Spiro denotes 2,2′,6,6′-tetrahydro-4H,4′H-5,5′-spirobi[cyclopenta-[c]pyrrole] cation.

We also compute vertical excitations for a variety of organic chromophores. All of these systems were included in a prior comparison between MC-PDFT and CASPT2.[15] We only consider singlet–singlet excitations in this work. We use the jul-cc-pVTZ basis set[33,34,40–42] for all valence excitations, the aug-cc-pVTZ basis set[33,34] for water, the 6-31+G** basis set[35–37] for *p*-nitroaniline (*p*NA) and 4-(dimethylamino)benzonitrile (DMABN), and the aug-

cc-pVDZ basis set[33,34] for the donor–acceptor complex of benzene (B) and tetracyanoethylene (TCNE). All vertical excitations are calculated using the SA-CASSCF ground-state geometry and were performed using C_1 symmetry. Additional information regarding the active space for each system is listed in Table 2.

Table 2: Systems for which vertical excitations are studied, number of states (N), number of active space electrons (n_e), number of active space orbitals (n_o), and description of active space orbitals.

System	N	(n_e, n_o)	Active Space
acetaldehyde	2	(12,12)	π, π^*, $2(n, n^*)$, σ_{CC}, σ^*_{CC}, σ_{CO}, σ^*_{CO}, σ_{CH}, σ^*_{CH}
acetone	2	(12,12)	π, π^*, $2(n, n^*)$, $2(\sigma_{CC}, \sigma^*_{CC})$, σ_{CO}, σ^*_{CO}
formaldehyde	2	(12,10)	full valence
pyrazine	3	(10,10)	$3(\pi, \pi^*)$, $2(n, n^*)$
pyridine	3	(8,8)	$3(\pi, \pi^*)$, n, n^*
pyrimidine	2	(10,10)	$3(\pi, \pi^*)$, $2(n, n^*)$
s-tetrazine	2	(14,14)	$3(\pi, \pi^*)$, $4(n, n^*)$
ethylene	3	(2,4)	π, π^*, 2 correlating π^*
butadiene	4	(10,10)	2π, $2\pi^*$, $3(\sigma_{CC}, \sigma^*_{CC})$
benzene	2	(6,13)	$3(\pi, \pi^*)$, $7\pi^*$
naphthalene	2	(10,10)	$5(\pi, \pi^*)$
furan	2	(6,10)	$2(\pi, \pi^*)$, (n, n^*), $4\pi^*$
hexatriene	2	(6,12)	$3(\pi, \pi^*)$, $6\pi^*$
water	2	(8,9)	$2(\sigma_{OH}, \sigma^*_{OH})$, $2(n, n^*)$, 3s
*p*NA[a]	3	(12,12)	$4(\pi, \pi^*)$, $2(n, n^*)$
DMABN[b]	3	(10,10)	$5(\pi, \pi^*)$
B-TCNE[c]	2	(4,4)	$2(\pi, \pi^*)$

[a] *p*-nitroaniline
[b] 4-(dimethylamino)benzonitrile
[c] donor–acceptor complex of benzene and tetracyanoethylene

All CMS-PDFT, MC-PDFT, and L-PDFT calculations were performed using *PySCF* (Version 2.1.1)[43,44] (commit 8ae2bb2eefc), *mrh*[45] (commit a4b9abd92f7), and *PySCF-forge*[46] (commit dd0d9f1b154). Geometry optimizations were performed with the *geomeTRIC*[47] plugin (version 1.0) for *PySCF*. The XMS-PDFT and XMS-CASPT2 calculations for acetylene were performed in *OpenMolcas* (Version 22.10)[48] (tag 462-g00b34a15f). All PDFT calculations used the tPBE functional. In *PySCF* a numerical quadrature grid size of 6 (80/120 radial and 770/974 angular for atoms of period 1/2 respectively) was used. In *OpenMolcas*,

the 'ultrafine' numerical quadrature grid (99 radial shells and 590 angular points for each atom, and a crowding factor of 10 and a fade factor of 10 for pruning angular grids) was used. For XMS-CASPT2, no ionization-potential-electron-affinity (IPEA)[49] shift was used, but an imaginary level shift of $0.3i$ was used. All L- and HL-PDFT calculations used the model space spanned by the SA-CASSCF eigenvectors to construct $\hat{H}^{\mathrm{L-PDFT}}$. All HMC-PDFT and HL-PDFT calculations used $\lambda = 0.25$ to correspond with the tPBE0 functional.

4 Results and Discussion

4.1 LiF

LiF has an avoided crossing between an ionic state and a covalent state and is widely used to test electronic structure methods.[50–59] Prior studies have shown that CMS-PDFT gives similar potential curves to XMS-CASPT2,[28] whereas MC- and HMC-PDFT display unphysical state crossings between 4 and 6 Å as well as a large dip in the potential curve for both states[26,27] (Figure 1). As can be seen in Figure 1, L-PDFT and HL-PDFT give the correct potential curve shape as well as the correct state ordering in this region, and neither method has the large dip in the potential curve at 4 Å.

4.2 LiH

LiH is another system that is widely studied to test new electronic structure methods.[60–66] We computed the four lowest $^1\Sigma$ states of LiH with both L-PDFT and HL-PDFT. The ground-state potential curves are presented in Figure S1. The three excited $^1\Sigma$ potential curves are presented in Figure 2.

CMS-PDFT is known to perform well for this system, getting close to XMS-CASPT2,[28] while MC-PDFT has an unphysical state crossing at 10 Å and a dip in the two highest states[27] (Figure 2). The figure shows that the L- and HL-PDFT calculations do not have dips in their potential curves at large Li-H internuclear distances, but they suffer from

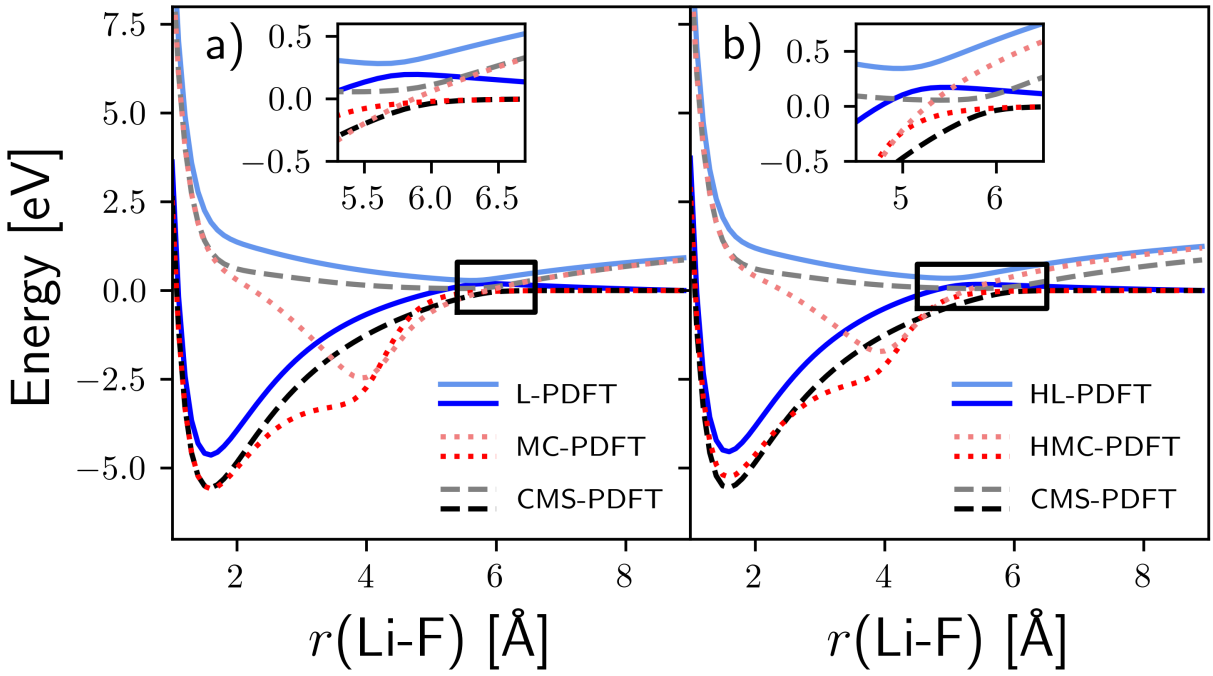

Figure 1: Potential energy curve of the two lowest states of LiF computed with CMS-PDFT, MC-PDFT, HMC-PDFT, L-PDFT, and HL-PDFT.

quantitative inaccuracy on the third state throughout the entire scan, with HL-PDFT being more quantitatively accurate.

4.3 Methylamine (CH_3NH_2)

Methylamine is a system whose photochemistry has been widely studied experimentally and theoretically.[67–82] Photodissociation of methylamine involves a conical intersection, and studying this process necessitates an electronic structure method that can appropriately describe the strong coupling between electronic states. Here, we study three N−H dissociation pathways of methylamine corresponding to the three torsional angles shown in Figure 3. CMS-PDFT has shown to give potential curves similar to those calculated by the much more expensive XMS-CASPT2 for all of these pathways.[28] The eclipsed geometry dissociation pathway passes very close to the conical intersection between the two states; whereas the 90° and 100° dissociations are further from the conical intersection yielding larger gaps

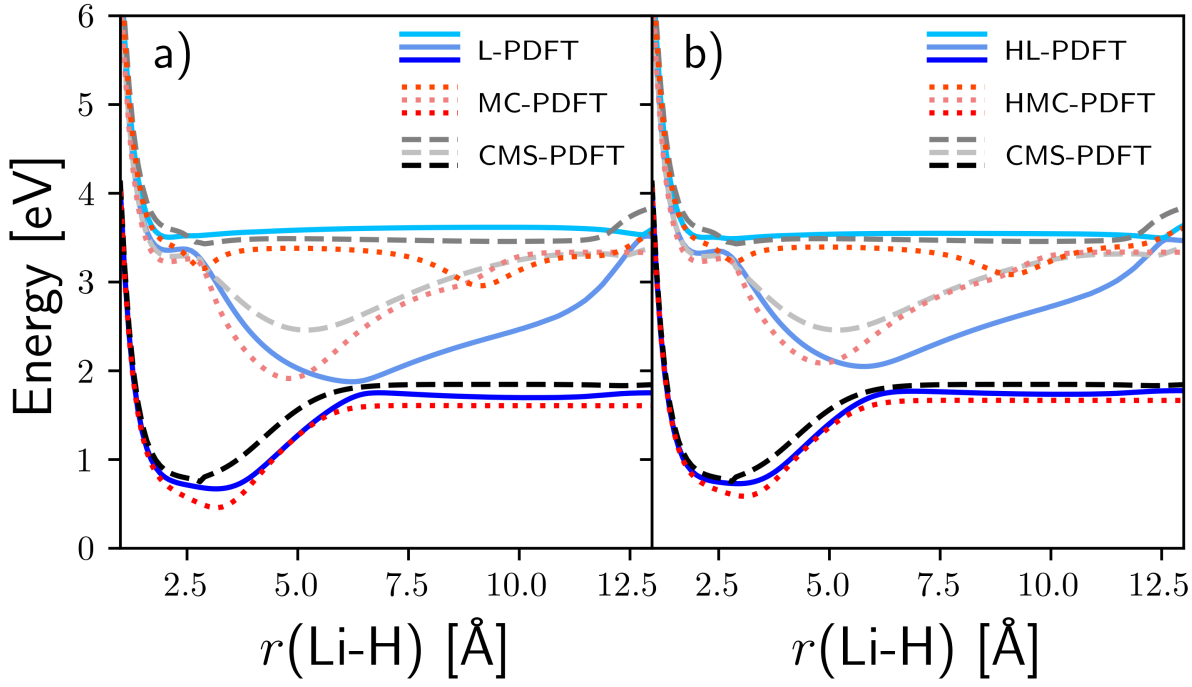

Figure 2: Potential energy curve for the 3 upper $^1\Sigma$ states of LiH computed with CMS-PDFT, MC-PDFT, HMC-PDFT, L-PDFT, and HL-PDFT. The ground state for each method is plotted in Figure S1.

between the states.

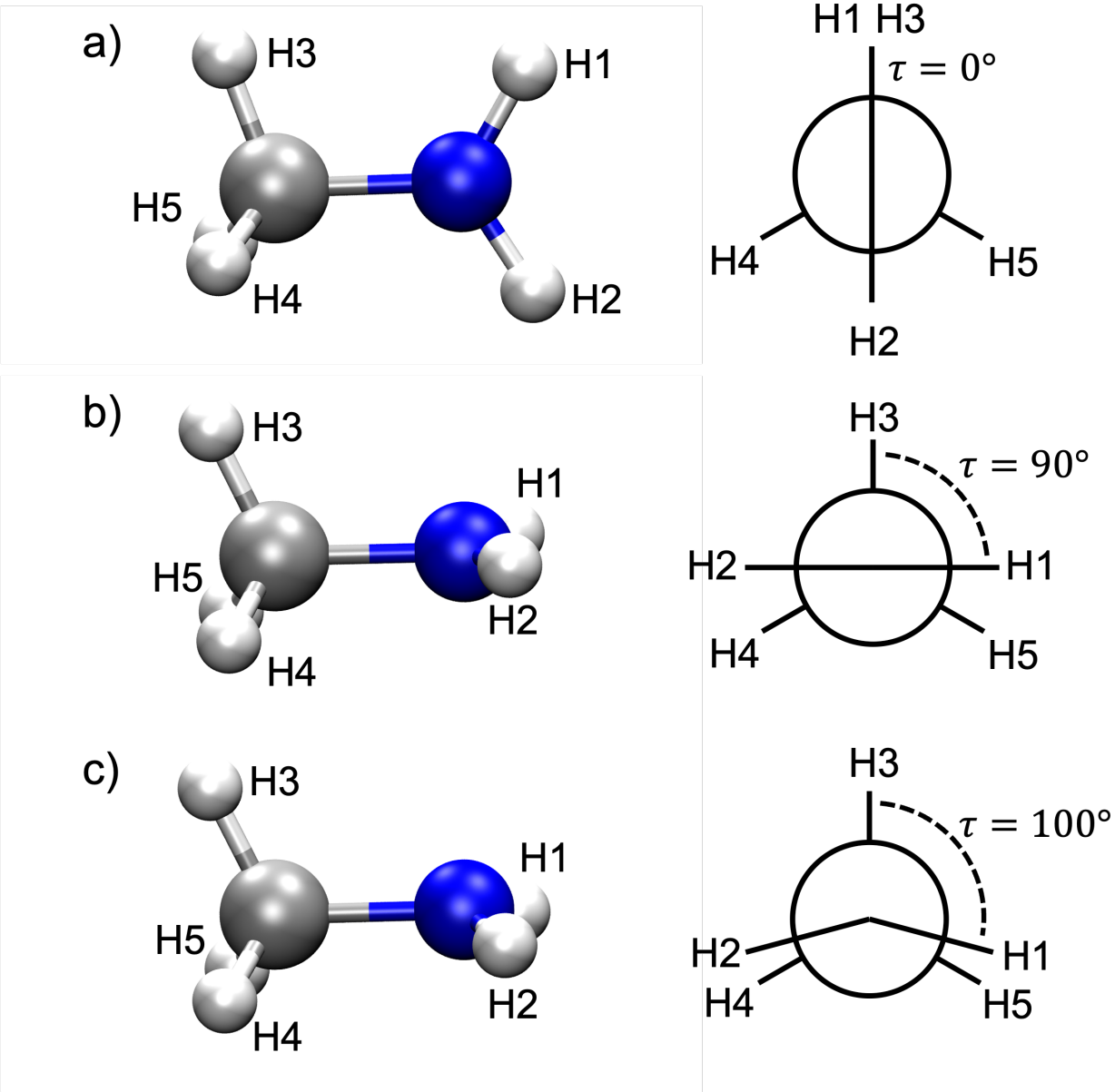

Figure 3: The lowest energy structure of methylamine for each torsional angle studied.

Figure 4 shows that that both L- and HL-PDFT are in excellent agreement with CMS-PDFT in the region of strong coupling for all three dihedral angles. Near the equilibrium structures (near the minimum of the ground-state PES), HL-PDFT is in good agreement with CMS-PDFT whereas L-PDFT differs.

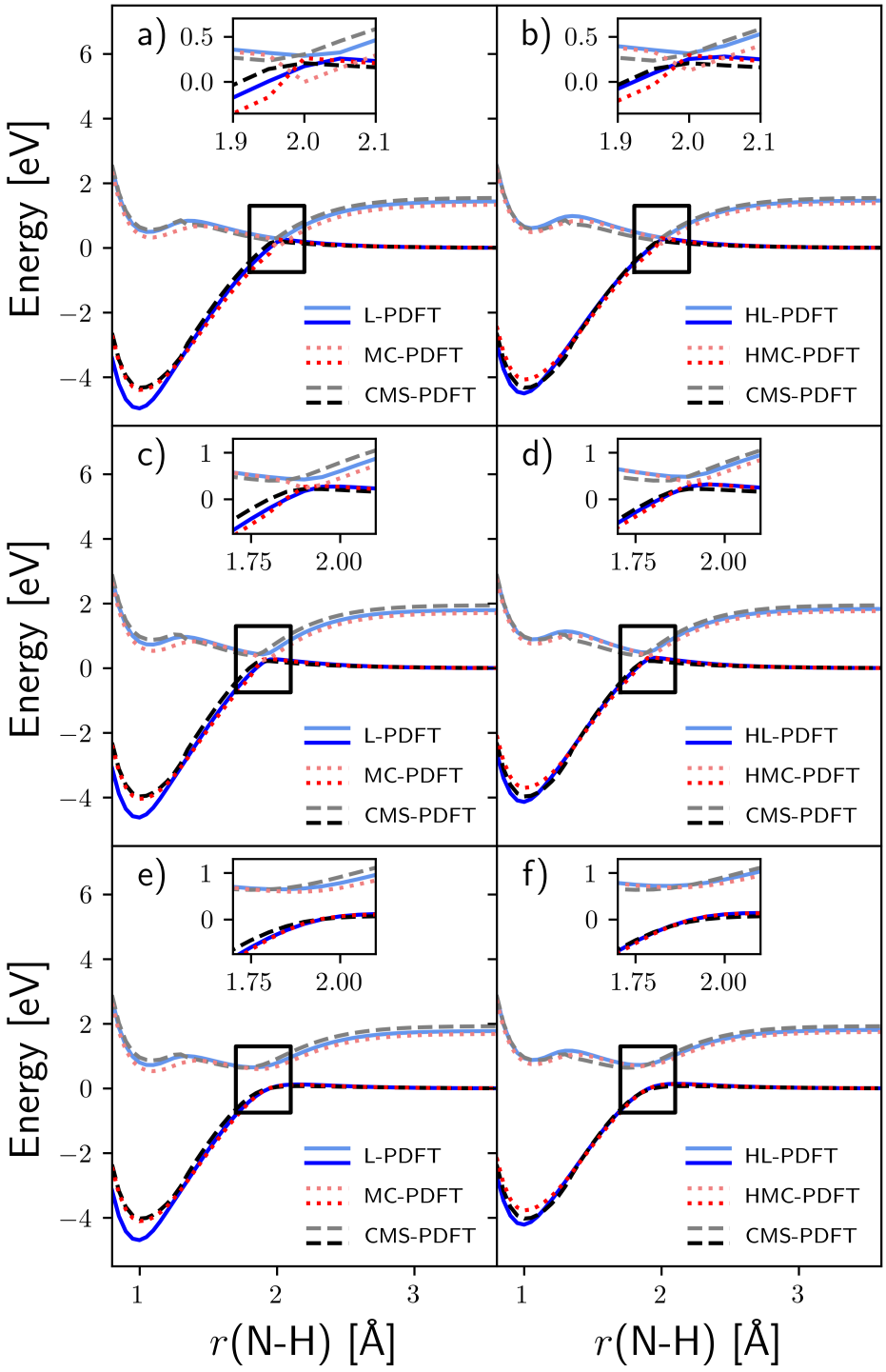

Figure 4: Potential energy curve of the two lowest states of methylamine computed with CMS-PDFT, MC-PDFT, HMC-PDFT, L-PDFT, and HL-PDFT for various fixed dihedrals τ. (a,b) $\tau = 0°$ or eclipsed. (c,d) $\tau = 90°$. (e,f) $\tau = 100°$.

4.4 Phenol (C_6H_5OH)

Phenol is a prototype of the $^1\pi\sigma^*$ motif that is common for a variety of biomolecules and aromatic molecules such as thiophenol.[83–91] As such, the photodissociation of phenol has been studied numerous times[88,92–98] making phenol a good model system to test whether a method can accurately construct the PES for photodissociation.

We consider two phenol photodissociations paths that differ in the C-C-O-H dihedral angle: $\varphi = 1°$ and $10°$. Figure 5 shows that L- and HL-PDFT are in good agreement with CMS-, MC-, and HMC-PDFT. The L- and HL-PDFT curves, like CMS-PDFT, have physically reasonable locally avoided crossings near the conical intersection along both photodissociation pathways.

4.5 Spiro Cation

The 2,2′,6,6′-tetrahydro-4H,4′H-5,5′-spirobi[cyclopenta-[c]pyrrole] cation, which we call the spiro cation, is a mixed-valence molecule with two subsystems that share a central, bridging carbon. Due to the Jahn-Teller effect, the cation hole is either partly localized on the left or right ring. The spiro cation structure is shown in Figure 6. Letting $\mathbf{R}^{(1)}$ and $\mathbf{R}^{(2)}$ denote the coordinates where the hole is localized on the left and right respectively, we consider a linear synchronous path from structure (1) $\rightarrow$ structure (2), and structures along the path given by

$$\mathbf{R}(\xi) = \left(\frac{1}{2} - \xi\right)\mathbf{R}^{(1)} + \left(\frac{1}{2} + \xi\right)\mathbf{R}^{(2)} \tag{18}$$

where ξ is a unitless reaction coordinate. The spiro cation is at an equilibrium geometry when $\xi = \pm 0.5$. For $\xi = 0$, an average of the two equilibrium structures is obtained, and this can be understood as the midpoint structure for intramolecular charge transfer. It has previously been shown that multireference perturbation theory can reasonable describe the PES only when going to the third order,[39,99,100] and this shows that the spiro cation a very difficult system to treat. CMS-PDFT has been shown to predict the correct PES topology,[28]

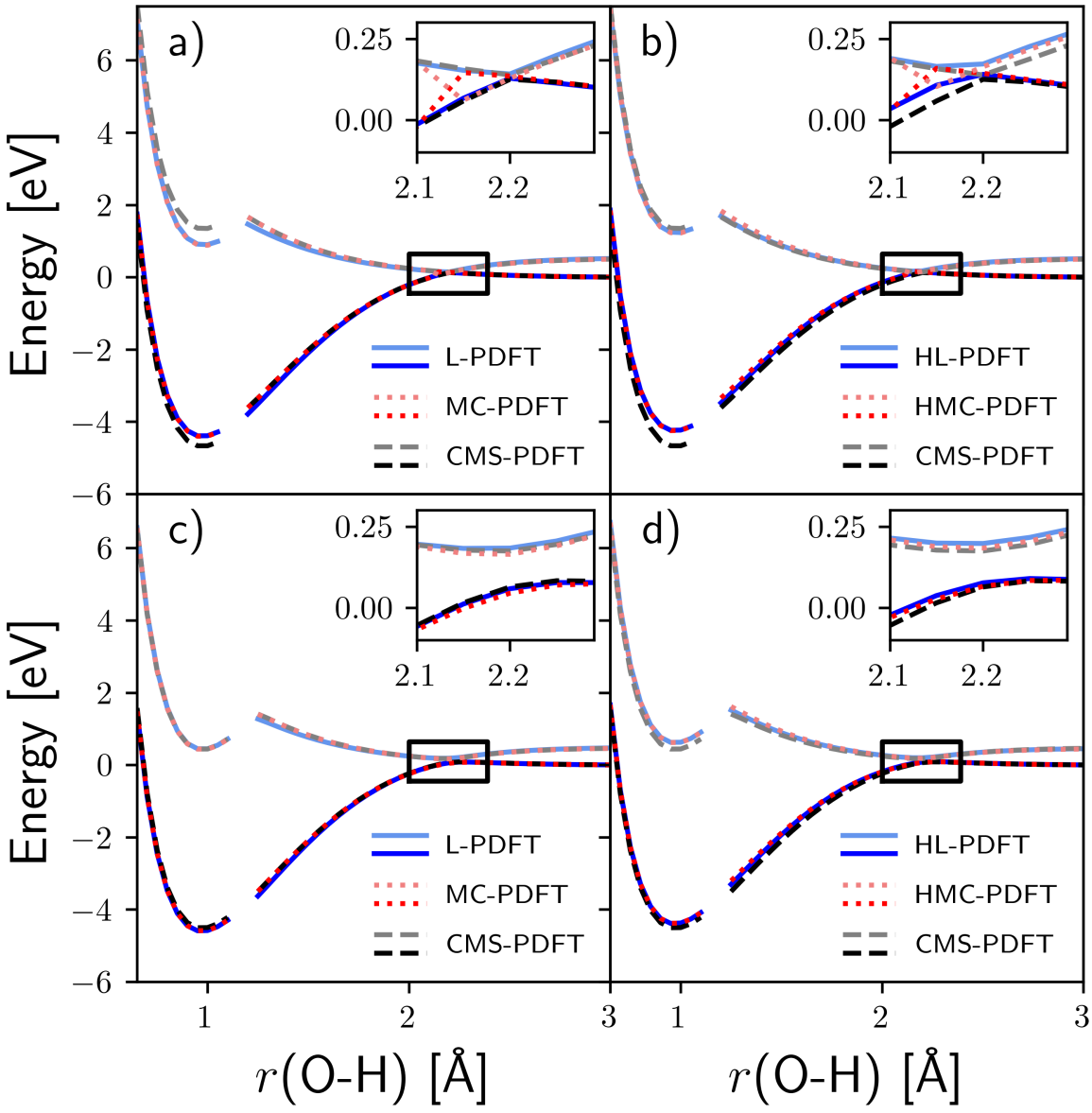

Figure 5: Potential energy curve of the two lowest states of phenol computed with CMS-PDFT, MC-PDFT, HMC-PDFT, L-PDFT, and HL-PDFT with a fixed dihedral φ. There is a gap in the potential energy curve due to an avoided crossing with a third state. (a,b) $\varphi = 1°$. (c,d) $\varphi = 10°$.

whereas XMS-PDFT and MC-PDFT fail in that they produce unphysical dips at $\xi = 0$[27] (Figure 7a).

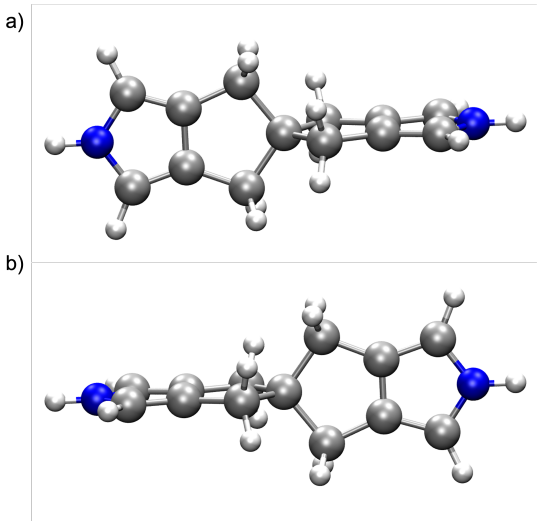

Figure 6: Two views of the 2,2',6,6'-tetrahydro-4H,4'H-5,5'-spirobi[cyclopenta-[c]pyrrole] (spiro) cation from the xz plane (a) and the yz plane (b).

The L-PDFT and HL-PDFT potential curves are shown in Figure 7. Like CMS-PDFT, these methods do not have a dip at the high symmetry point $\xi = 0$, as is present in the MC-PDFT, HMC-PDFT, and XMS-PDFT potential curves[27] (Figure 7). In fact, L-PDFT and HL-PDFT hardly differ at all from CMS-PDFT, even at the high-symmetry point, giving good quantitative agreement between the methods. Furthermore, the coupling term between these two states ($H_{01}^{\mathrm{L-PDFT}}$) goes to zero as the molecule approaches the midpoint structure ($\xi \to 0$) (Figure S2), indicating that $\hat{H}^{\mathrm{L-PDFT}}$ maintains the correct physical charge transfer symmetry at that point.

4.6 Acetylene (C_2H_2)

We now consider acetylene, a linear system with degenerate $^1\Delta_u$ excited states at its ground-state equilibrium geometry. We consider the four lowest valence excited singlet states of acetylene as a function of one of the C-C-H bond angles (defined to be θ where $\theta = 180°$ is the linear geometry (the other C-C-H angle is kept linear). An introduction to the energetics,

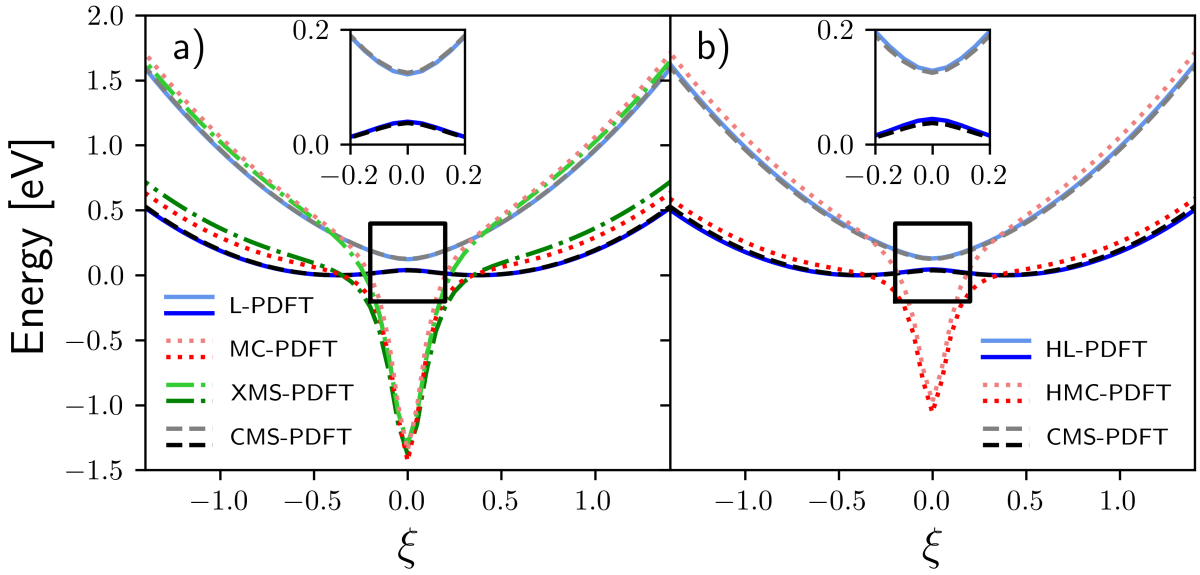

Figure 7: Potential energy curves of the two lowest states of the spiro cation computed with CMS-PDFT, XMS-PDFT, MC-PDFT, HMC-PDFT, L-PDFT, and HL-PDFT. XMS-PDFT data taken from Ref 28.

symmetries, and geometry dependence of these states is provided in articles by Cui et al.[101] and Ventura et al.[102] The symmetries of these states for planar, nonlinear geometries are $^1A'$, $^1A''$, $^1A'$, and $^1A''$, in order of increasing energy. For linear geometries, they become $^1\Sigma_g^+$, $^1\Sigma_u^-$, and two components of a $^1\Delta_u$ state. Our goal here is to test the accuracy of L-PDFT on this system for which CMS-PDFT is known to provide an incorrect description of the degenerate $^1\Delta_u$ states at $\theta = 180°$.

Our CMS-PDFT calculations are unable to compute the energy at $\theta = 180°$ due to the intermediate-state optimization not converging, so we omit this point and only consider θ between 135° and 179°. Figure 8 shows the three excited singlet states for all the methods considered, with the zero of energy set to the first excited state at $\theta = 179°$. The upper states should become doubly degenerate $^1\Delta_u$ states as $\theta \to 180°$, and that is clearly seen for XMS-CASPT2 and XMS-PDFT, although the upper $^1\Delta_u$ potential of XMS-PDFT has the wrong curvature around 160°. The CMS-PDFT $^1\Delta_u$ states, however, incorrectly remain split as $\theta \to 180°$ (Figure 8a). The ground-state potential curves are almost identical for

all the methods except for CMS-PDFT, which has a discontinuity at $\theta = 179°$ (Figure S3). This discontinuity likely results from the structure being too close to the linear structure, and thus the intermediate state optimization is struggling.

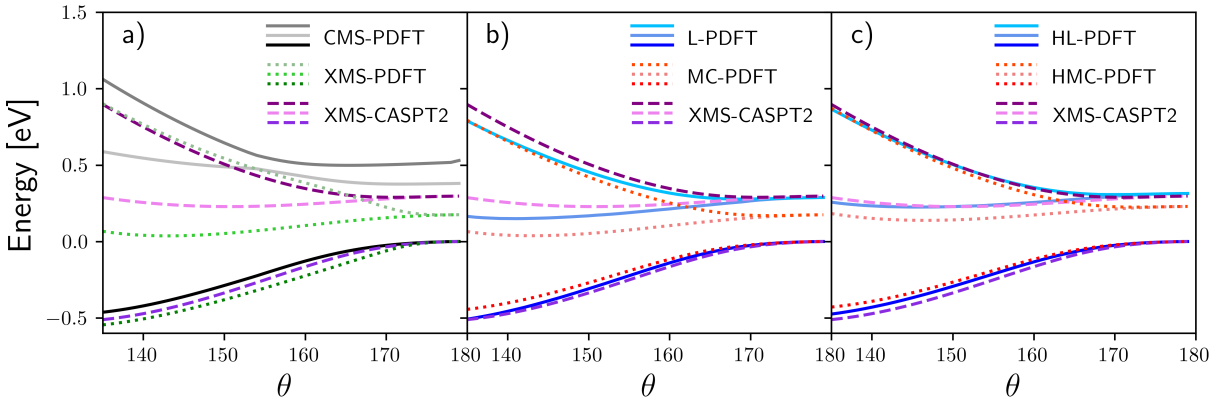

Figure 8: Potential energy curves of the three lowest excited singlet states of acetylene (the states that become $^1\Sigma_u^-$ and two components of $^1\Delta_u$ at linear geometries) computed with XMS-CASPT2, XMS-PDFT, CMS-PDFT, MC-PDFT, HMC-PDFT, L-PDFT, and HL-PDFT. The zero of energy is taken as the energy of the first excited singlet state at $\theta = 179°$. The ground-state potential energy curves for these methods are plotted in Figure S3.

Figure 8b shows that L-PDFT and MC-PDFT PESs are in excellent agreement with XMS-CASPT2; correctly reproducing the degenerate $^1\Delta_u$ states as $\xi \to 0$. Figure S4 shows the excited states of all the methods with the zero of energy set to the ground state minimum energy to highlight the difference in vertical excitation energies from the ground state. That figure shows that all the methods produce different vertical excitation energies such that all the PDFT methods except CMS-PDFT have lower excitation energies for $^1\Sigma_u^-$ and $^1\Delta_u$ states than does XMS-CASPT2. The CMS-PDFT method, despite its inability to recover the degenerate $^1\Delta_u$ states, yields vertical gaps in good agreement with XMS-CASPT2 except for the uppermost $^1\Delta_u$ state.

4.7 Vertical Excitation Benchmarking

Here we test the quantitative accuracy of L-PDFT vertical excitation energies for a variety of organic chromophores which have been studied previously with MC-PDFT and CASPT2.[15] Our test set includes the lowest-energy spin-conserving valence excitation energies of 13 organic molecules (acetaldehyde, acetone, formaldehyde, pyrazine, pyridine, pyrimidine, *s*-tetrazine, ethylene, butadiene, benzene, naphthalene, furan, and hexatriene). We also test one Rydberg state: the lowest singlet excitation of water. In addition, we also include energies for *p*NA and DMABN intramolecular charge transfer excitations, as well as the B-TCNE intermolecular charge transfer excitation.

Table 3 summarizes the vertical excitation energies for all of the systems. CASSCF, which lacks external correlation (dynamic correlation outside of the active space), performs poorly compared to the other methods, with an overall mean unsigned error (MUE) of 0.57 eV. Considering the valence excitations first, CMS-PDFT has a larger MUE as compared to MC-PDFT, and the hybrid methods HMC- and HL-PDFT perform similarly to MC-PDFT. L-PDFT performs the best of all the methods for valence excitations with a MUE of 0.24 eV.

For the Rydberg excitation of water, all of the methods perform similarly, with almost no error in the vertical excitation energy in comparison to the reference value.

Finally, for the charge transfer excitations, CMS-PDFT again performs worse than MC-PDFT for these test systems with a substantially higher MUE of 0.27 eV whereas L-PDFT and MC-PDFT have very small MUEs of 0.09 and 0.08 eV respectively. HL-PDFT has a slightly worse MUE of 0.11 eV. The performance of HMC-PDFT is between that of HL-PDFT and CMS-PDFT.

If we consider all of the excitations, L-PDFT performs the best with a MUE of 0.20 eV followed by MC-PDFT with a MUE of 0.24 eV. CMS-PDFT performs worse than both MC-PDFT and L-PDFT for these vertical excitations with an overall MUE of 0.39 eV. For both pyrimidine and *s*-tetrazine, CMS-PDFT agrees with CASSCF, which performs poorly

Table 3: Vertical excitation energies (in eV) for organic chromophores calculated with SA-CASSCF, MC-PDFT, HMC-PDFT, L-PDFT, HL-PDFT, and CMS-PDFT. Details about the active space and state averaging are listed in Table 2. MSE: mean signed error. MUE: mean unsigned error. CT: charge transfer

System	Excited State	CASSCF	MC-PDFT	HMC-PDFT	L-PDFT	HL-PDFT	CMS-PDFT	Reference
acetaldehyde	$^1A''$ $n \rightarrow \pi^*$	4.11	4.19	4.17	4.19	4.17	4.19	4.28[103]
acetone	$^1A_2$ $n \rightarrow \pi^*$	4.56	4.38	4.43	4.39	4.43	4.38	4.43[103]
formaldehyde	$^1A_2$ $n \rightarrow \pi^*$	4.22	3.96	4.02	3.98	4.04	4.22	4.00[103]
pyrazine	$^1B_{3u}$ $n \rightarrow \pi^*$	5.10	3.95	4.24	3.88	4.19	4.50	3.97[104,105]
pyridine	$^1B_1$ $n \rightarrow \pi^*$	5.66	5.06	5.21	4.96	5.13	4.88	4.74[106,107]
pyrimidine	$^1B_1$ $n \rightarrow \pi^*$	4.99	4.34	4.50	4.34	4.50	4.99	4.18[108]
s-tetrazine	$^1B_{3u}$ $n \rightarrow \pi^*$	3.82	2.69	2.97	2.70	2.98	3.82	2.25[103]
ethylene	$^1B_{1u}$ $\pi \rightarrow \pi^*$	8.00	7.26	7.45	7.92	7.93	8.03	8.02[109]
butadiene	^1B_u $\pi \rightarrow \pi^*$	6.41	6.19	6.25	6.20	6.25	7.06	6.21[110]
benzene	$^1B_{2u}$ $\pi \rightarrow \pi^*$	5.00	5.21	5.16	5.21	5.16	5.00	4.90[111]
naphthalene	$^1B_{3u}$ $\pi \rightarrow \pi^*$	4.31	4.49	4.44	4.49	4.44	4.31	4.00[112]
furan	$^1B_2$ $\pi \rightarrow \pi^*$	6.69	6.55	6.59	6.59	6.61	6.49	6.06[113]
hexatriene	^1B_u $\pi \rightarrow \pi^*$	5.61	5.53	5.55	5.53	5.55	5.55	4.93[114]
water	Singlet, $2p_x \rightarrow 3s$	7.40	7.38	7.39	7.39	7.39	7.38	7.40[115]
*p*NA	$^1A_1$ $\pi \rightarrow \pi^*$	4.76	4.35	4.45	4.28	4.40	4.24	4.30[15]
DMABN	$^1A_1$ $\pi \rightarrow \pi^*$	6.54	4.56	5.05	4.56	4.75	5.15	4.57[116]
B-TCNE	^1A $\pi \rightarrow \pi^*$	4.02	3.37	3.53	3.37	3.53	3.43	3.59[117]
MSE Valence		-0.50	-0.14	-0.23	-0.18	-0.26	-0.42	
MUE Valence		0.53	0.29	0.34	0.24	0.29	0.44	
MSE CT		-0.95	0.06	-0.19	0.08	-0.07	-0.12	
MUE CT		0.95	0.09	0.23	0.08	0.11	0.27	
MSE		-0.55	-0.10	-0.21	-0.13	-0.21	-0.34	
MUE		0.57	0.24	0.30	0.20	0.24	0.39	

at describing these transitions (Table 3). We see that L-PDFT corrects the MC-PDFT vertical excitation for ethylene (MC-PDFT greatly underestimates this excitation). In most cases though, L-PDFT yields similar excitation energies to MC-PDFT, although it is still unknown how L-PDFT will perform when considering a larger number of states ($N > 5$), and when the number of states whose density matrices are averaged in the of the model space grows. Regardless, it is very encouraging that on this small but representative set of organic molecules, L-PDFT performs as well as MC-PDFT at predicting the vertical excitations.

5 Conclusion

In contrast to previous MS-PDFT methods that define the diagonal and off-diagonal effective Hamiltonian matrix elements by separate theories, L-PDFT defines an effective Hamiltonian operator as a functional of a model space *via* the state-averaged density matrices within that space.

$$\hat{H}^{\mathrm{L-PDFT}}[\rho[\mathbf{D}^0[\mathscr{U}]], \Pi[\mathbf{d}^0[\mathscr{U}]]] = \hat{H}^{\mathrm{L-PDFT}}[\mathscr{U}] \tag{19}$$

$\hat{H}^{\mathrm{L-PDFT}}[\mathscr{U}]$ is constructed such that its expectation value for any state yields a linear approximation to the MC-PDFT energy of that state around the state-averaged densities. Diagonalization of $\hat{H}^{\mathrm{L-PDFT}}[\mathscr{U}]$ yields PESs that have the correct topology near conical intersections and locally avoided crossings, a property that is also enforced in other MS-PDFT methods such as CMS-PDFT. Unlike XMS-PDFT, L-PDFT is able to correctly reproduce the PES for the difficult spiro cation. Additionally, L-PDFT does not fail for degenerate states of nearly-linear molecules as CMS-PDFT does. Benchmarking L-PDFT vertical excitation energies for a representative set of organic chromophores showed that L-PDFT performs similarly to MC-PDFT, whereas CMS-PDFT performs worse than MC-PDFT. Further, we note that the computational cost of L-PDFT scales as a constant with the number of states included in the state averaging, whereas MC-PDFT and CMS-PDFT scale linearly with the number of states, making L-PDFT formally a faster method. Lastly, L-PDFT also has the

advantage of having a well-defined Hamiltonian-like operator which prior MS-PDFT and MC-PDFT do not have.

Supporting Information Available

Structure coordinates, absolute energies for PES scans, LiH ground-state potential energy curve, L-PDFT Hamiltonian coupling elements for the spiro cation, acetylene ground and excited-state potential energy curves. This information is available free of charge.

Acknowledgement

The authors acknowledge helpful discussions with Jie J. Bao. This work was supported in part by the National Science Foundation under grant CHE-2054723. We also acknowledge the University of Chicago's Research Computing Center for their support of this work.

References

(1) Michl, J.; Bonačić-Koutecký, V. *Electronic Aspects of Organic Photochemistry*; Wiley-Interscience: Chichester, 1990.

(2) Balzani, V.; Ceroni, P.; Juris, A. *Photochemistry and Photophysics: Concepts, Research, Applications*; Wiley-VCH: Weinheim, Germany, 2014.

(3) Proppe, A. H. et al. Bioinspiration in Light Harvesting and Catalysis. *Nat. Rev. Mater.* **2020**, *5*, 828–846.

(4) Croce, R.; van Amerongen, H. Light Harvesting in Oxygenic Photosynthesis: Structural Biology Meets Spectroscopy. *Science* **2020**, *369*, eaay2058.

(5) McCusker, J. K. Electronic Structure in the Transition Metal Block and Its Implications for Light Harvesting. *Science* **2019**, *363*, 484–488.

(6) Herrmann, J.-M. *Kirk-Othmer Encyclopedia of Chemical Technology*; Wiley: New York, 2017; pp 1–44.

(7) Kilin, D., Kilina, S. V., Han, Y., Eds. *Computational Photocatalysis: Modeling of Photophysics and Photochemistry at Interfaces*; ACS Symposium Series 1331; American Chemical Society: Washington, DC, 2019.

(8) Richards, B. S.; Hudry, D.; Busko, D.; Turshatov, A.; Howard, I. A. Photon Upconversion for Photovoltaics and Photocatalysis: A Critical Review. *Chem. Rev.* **2021**, *121*, 9165–9195.

(9) Losi, A.; Gärtner, W. A Light Life Together: Photosensing in the Plant Microbiota. *Photochem. Photobiol. Sci.* **2021**, *20*, 451–473.

(10) Wand, A.; Gdor, I.; Zhu, J.; Sheves, M.; Ruhman, S. Shedding New Light on Retinal Protein Photochemistry. *Annu. Rev. Phys. Chem.* **2013**, *64*, 437–458.

(11) Kandori, H. Retinal Proteins: Photochemistry and Optogenetics. *BCSJ* **2020**, *93*, 76–85.

(12) Marchetti, B.; V. Karsili, T. N.; R. Ashfold, M. N.; Domcke, W. A 'Bottom up', Ab Initio Computational Approach to Understanding Fundamental Photophysical Processes in Nitrogen Containing Heterocycles, DNA Bases and Base Pairs. *Phys. Chem. Chem. Phys.* **2016**, *18*, 20007–20027.

(13) May, V.; Kühn, O. *Charge and Energy Transfer Dynamics in Molecular Systems*; Wiley-VCH: Berlin, 2000.

(14) Li Manni, G.; Carlson, R. K.; Luo, S.; Ma, D.; Olsen, J.; Truhlar, D. G.; Gagliardi, L. Multiconfiguration Pair-Density Functional Theory. *J. Chem. Theory Comput.* **2014**, *10*, 3669–3680.

(15) Hoyer, C. E.; Ghosh, S.; Truhlar, D. G.; Gagliardi, L. Multiconfiguration Pair-Density Functional Theory Is as Accurate as CASPT2 for Electronic Excitation. *J. Phys. Chem. Lett.* **2016**, *7*, 586–591.

(16) King, D. S.; Hermes, M. R.; Truhlar, D. G.; Gagliardi, L. Large-Scale Benchmarking of Multireference Vertical-Excitation Calculations via Automated Active-Space Selection. *J. Chem. Theory Comput.* **2022**, *18*, 6065–6076.

(17) Pandharkar, R.; Hermes, M. R.; Truhlar, D. G.; Gagliardi, L. A New Mixing of Nonlocal Exchange and Nonlocal Correlation with Multiconfiguration Pair-Density Functional Theory. *J. Phys. Chem. Lett.* **2020**, *11*, 10158–10163.

(18) Angeli, C.; Cimiraglia, R.; Evangelisti, S.; Leininger, T.; Malrieu, J.-P. Introduction of N-Electron Valence States for Multireference Perturbation Theory. *J. Chem. Phys.* **2001**, *114*, 10252–10264.

(19) Lischka, H.; Nachtigallová, D.; Aquino, A. J. A.; Szalay, P. G.; Plasser, F.; Machado, F. B. C.; Barbatti, M. Multireference Approaches for Excited States of Molecules. *Chem. Rev.* **2018**, *118*, 7293–7361.

(20) Finley, J.; Malmqvist, P.-Å.; Roos, B. O.; Serrano-Andrés, L. The Multi-State CASPT2 Method. *Chem. Phys. Lett.* **1998**, *288*, 299–306.

(21) Shiozaki, T.; Győrffy, W.; Celani, P.; Werner, H.-J. Communication: Extended Multi-State Complete Active Space Second-Order Perturbation Theory: Energy and Nuclear Gradients. *J. Chem. Phys.* **2011**, *135*, 081106.

(22) Nakano, H. Quasidegenerate Perturbation Theory with Multiconfigurational Self-consistent-field Reference Functions. *J. Chem. Phys.* **1993**, *99*, 7983–7992.

(23) Angeli, C.; Borini, S.; Cestari, M.; Cimiraglia, R. A Quasidegenerate Formulation of

the Second Order N-Electron Valence State Perturbation Theory Approach. *J. Chem. Phys.* **2004**, *121*, 4043–4049.

(24) Granovsky, A. A. Extended Multi-Configuration Quasi-Degenerate Perturbation Theory: The New Approach to Multi-State Multi-Reference Perturbation Theory. *J. Chem. Phys.* **2011**, *134*, 214113.

(25) Szalay, P. G.; Müller, T.; Gidofalvi, G.; Lischka, H.; Shepard, R. Multiconfiguration Self-Consistent Field and Multireference Configuration Interaction Methods and Applications. *Chem. Rev.* **2012**, *112*, 108–181.

(26) Sand, A. M.; Hoyer, C. E.; Truhlar, D. G.; Gagliardi, L. State-Interaction Pair-Density Functional Theory. *J. Chem. Phys.* **2018**, *149*, 024106.

(27) J. Bao, J.; Zhou, C.; Varga, Z.; Kanchanakungwankul, S.; Gagliardi, L.; G. Truhlar, D. Multi-State Pair-Density Functional Theory. *Faraday Discuss.* **2020**, *224*, 348–372.

(28) Bao, J. J.; Zhou, C.; Truhlar, D. G. Compressed-State Multistate Pair-Density Functional Theory. *J. Chem. Theory Comput.* **2020**, *16*, 7444–7452.

(29) Bao, J. J.; Hermes, M. R.; Scott, T. R.; Sand, A. M.; Lindh, R.; Gagliardi, L.; Truhlar, D. G. Analytic Gradients for Compressed Multistate Pair-Density Functional Theory. *Molecular Physics* **2022**, e2110534.

(30) Sand, A. M.; Hoyer, C. E.; Sharkas, K.; Kidder, K. M.; Lindh, R.; Truhlar, D. G.; Gagliardi, L. Analytic Gradients for Complete Active Space Pair-Density Functional Theory. *J. Chem. Theory Comput.* **2018**, *14*, 126–138.

(31) Scott, T. R.; Hermes, M. R.; Sand, A. M.; Oakley, M. S.; Truhlar, D. G.; Gagliardi, L. Analytic Gradients for State-Averaged Multiconfiguration Pair-Density Functional Theory. *J. Chem. Phys.* **2020**, *153*, 1–12.

(32) Becke, A. D. A New Mixing of Hartree–Fock and Local Density-functional Theories. *J. Chem. Phys.* **1993**, *98*, 1372–1377.

(33) Dunning, T. H. Gaussian Basis Sets for Use in Correlated Molecular Calculations. I. The Atoms Boron through Neon and Hydrogen. *J. Chem. Phys.* **1989**, *90*, 1007–1023.

(34) Kendall, R. A.; Dunning, T. H.; Harrison, R. J. Electron Affinities of the First-row Atoms Revisited. Systematic Basis Sets and Wave Functions. *J. Chem. Phys.* **1992**, *96*, 6796–6806.

(35) Frisch, M. J.; Pople, J. A.; Binkley, J. S. Self-consistent Molecular Orbital Methods 25. Supplementary Functions for Gaussian Basis Sets. *J. Chem. Phys.* **1984**, *80*, 3265–3269.

(36) Krishnan, R.; Binkley, J. S.; Seeger, R.; Pople, J. A. Self-consistent Molecular Orbital Methods. XX. A Basis Set for Correlated Wave Functions. *J. Chem. Phys.* **1980**, *72*, 650–654.

(37) Hehre, W. J.; Ditchfield, R.; Pople, J. A. Self—Consistent Molecular Orbital Methods. XII. Further Extensions of Gaussian—Type Basis Sets for Use in Molecular Orbital Studies of Organic Molecules. *J. Chem. Phys.* **1972**, *56*, 2257–2261.

(38) Hariharan, P. C.; Pople, J. A. The Influence of Polarization Functions on Molecular Orbital Hydrogenation Energies. *Theoret. Chim. Acta* **1973**, *28*, 213–222.

(39) Dong, S. S.; Huang, K. B.; Gagliardi, L.; Truhlar, D. G. State-Interaction Pair-Density Functional Theory Can Accurately Describe a Spiro Mixed Valence Compound. *J. Phys. Chem. A* **2019**, *123*, 2100–2106.

(40) Feller, D. The Role of Databases in Support of Computational Chemistry Calculations. *J. Comput. Chem.* **1996**, *17*, 1571–1586.

(41) Schuchardt, K. L.; Didier, B. T.; Elsethagen, T.; Sun, L.; Gurumoorthi, V.; Chase, J.; Li, J.; Windus, T. L. Basis Set Exchange: A Community Database for Computational Sciences. *J. Chem. Inf. Model.* **2007**, *47*, 1045–1052.

(42) Papajak, E.; Truhlar, D. G. Convergent Partially Augmented Basis Sets for Post-Hartree-Fock Calculations of Molecular Properties and Reaction Barrier Heights. *J. Chem. Theory Comput.* **2011**, *7*, 10–18.

(43) Sun, Q.; Berkelbach, T. C.; Blunt, N. S.; Booth, G. H.; Guo, S.; Li, Z.; Liu, J.; McClain, J. D.; Sayfutyarova, E. R.; Sharma, S.; Wouters, S.; Chan, G. K.-L. PySCF: The Python-based Simulations of Chemistry Framework. *WIREs Comput. Mol. Sci.* **2018**, *8*, e1340.

(44) Sun, Q. et al. Recent Developments in the PySCF Program Package. *J. Chem. Phys.* **2020**, *153*, 024109.

(45) Hermes, M. R. mrh. 2018; `https://github.com/MatthewRHermes/mrh`.

(46) Pyscf-Forge. 2022; `https://github.com/pyscf/pyscf-forge`.

(47) Wang, L.-P.; Song, C. Geometry Optimization Made Simple with Translation and Rotation Coordinates. *J. Chem. Phys.* **2016**, *144*, 214108.

(48) Fdez. Galván, I. et al. OpenMolcas: From Source Code to Insight. *J. Chem. Theory Comput.* **2019**, *15*, 5925–5964.

(49) Ghigo, G.; Roos, B. O.; Malmqvist, P.-Å. A Modified Definition of the Zeroth-Order Hamiltonian in Multiconfigurational Perturbation Theory (CASPT2). *Chem. Phys. Lett.* **2004**, *396*, 142–149.

(50) Kahn, L. R.; Hay, P. J.; Shavitt, I. Theoretical Study of Curve Crossing: Ab Initio Calculations on the Four Lowest 1Σ+ States of LiF. *J. Chem. Phys.* **1974**, *61*, 3530–3546.

(51) Botter, B. J.; Kooter, J. A.; Mulder, J. J. C. Ab-Initio Calculations of the Covalent-Ionic Curve Crossing in LiF. *Chem. Phys. Lett.* **1975**, *33*, 532–534.

(52) Werner, H.-J.; Meyer, W. MCSCF Study of the Avoided Curve Crossing of the Two Lowest 1Σ+ States of LiF. *J. Chem. Phys.* **1981**, *74*, 5802–5807.

(53) Finley, J. P.; Witek, H. A. Diagrammatic Complete Active Space Perturbation Theory: Calculations on Benzene, N2, and LiF. *J. Chem. Phys.* **2000**, *112*, 3958–3963.

(54) Nakamura, H.; Truhlar, D. G. Direct Diabatization of Electronic States by the Fourfold Way. II. Dynamical Correlation and Rearrangement Processes. *J. Chem. Phys.* **2002**, *117*, 5576–5593.

(55) Meller, J.; Malrieu, J.-P.; Heully, J.-L. Size-Consistent Multireference Configuration Interaction Method through the Dressing of the Norm of Determinants. *Mol. Phys.* **2003**, *101*, 2029–2041.

(56) Legeza, Ö.; Röder, J.; Hess, B. A. QC-DMRG Study of the Ionic-Neutral Curve Crossing of LiF. *Mol. Phys.* **2003**, *101*, 2019–2028.

(57) Angeli, C.; Cimiraglia, R.; Malrieu, J.-P. A Simple Approximate Perturbation Approach to Quasi-Degenerate Systems. *Theor. Chem. Acc.* **2006**, *116*, 434–439.

(58) Hanrath, M. Multi-Reference Coupled-Cluster Study of the Ionic-Neutral Curve Crossing LiF. *Mol. Phys.* **2008**, *106*, 1949–1957.

(59) Li, C.; Lindh, R.; Evangelista, F. A. Dynamically Weighted Multireference Perturbation Theory: Combining the Advantages of Multi-State and State-Averaged Methods. *J. Chem. Phys.* **2019**, *150*, 144107.

(60) Fallon, R. J.; Vanderslice, J. T.; Mason, E. A. Potential Energy Curves for Lithium Hydride. *J. Chem. Phys.* **1960**, *32*, 1453–1455.

(61) Li, K. C.; Stwalley, W. C. The A 1Σ+ → X 1Σ+ Bands of the Isotopic Lithium Hydrides. *J. Mol. Spectrosc.* **1978**, *69*, 294–318.

(62) Pardo, A.; Camacho, J. J.; Poyato, J. M. L. The Padé-Approximant Method and Its Applications in the Construction of Potential-Energy Curves for the Lithium Hydride Molecule. *Chem. Phys. Lett.* **1986**, *131*, 490–495.

(63) Stwalley, W. C.; Zemke, W. T. Spectroscopy and Structure of the Lithium Hydride Diatomic Molecules and Ions. *J. Phys. Chem. Ref. Data* **1993**, *22*, 87–112.

(64) Nakamura, H.; Truhlar, D. G. The Direct Calculation of Diabatic States Based on Configurational Uniformity. *J. Chem. Phys.* **2001**, *115*, 10353–10372.

(65) Hoyer, C. E.; Parker, K.; Gagliardi, L.; Truhlar, D. G. The DQ and DQΦ Electronic Structure Diabatization Methods: Validation for General Applications. *J. Chem. Phys.* **2016**, *144*, 194101.

(66) Grofe, A.; Qu, Z.; Truhlar, D. G.; Li, H.; Gao, J. Diabatic-At-Construction Method for Diabatic and Adiabatic Ground and Excited States Based on Multistate Density Functional Theory. *J. Chem. Theory Comput.* **2017**, *13*, 1176–1187.

(67) Michael, J. V.; Noyes, W. A. The Photochemistry of Methylamine. *J. Am. Chem. Soc.* **1963**, *85*, 1228–1233.

(68) Kassab, E.; Gleghorn, J. T.; Evleth, E. M. Theoretical Aspects of the Photochemistry of Methanol, Methylamine, and Related Materials. *J. Am. Chem. Soc.* **1983**, *105*, 1746–1753.

(69) Waschewsky, G. C. G.; Kitchen, D. C.; Browning, P. W.; Butler, L. J. Competing Bond Fission and Molecular Elimination Channels in the Photodissociation of CH3NH2 at 222 Nm. *J. Phys. Chem.* **1995**, *99*, 2635–2645.

(70) Reed, C. L.; Kono, M.; Ashfold, M. N. R. Near-UV Photolysis of Methylamine Studied by H-atom Photofragment Translational Spectroscopy. *J. Chem. Soc., Faraday Trans.* **1996**, *92*, 4897–4904.

(71) Dunn, K. M.; Morokuma, K. Ab Initio Study of the Photochemical Dissociation of Methylamine. *J. Phys. Chem.* **1996**, *100*, 123–129.

(72) Baek, S. J.; Choi, K.-W.; Choi, Y. S.; Kim, S. K. Spectroscopy and Dynamics of Methylamine. I. Rotational and Vibrational Structures of CH3NH2 and CH3ND2 in $\tilde{A}$ States. *J. Chem. Phys.* **2003**, *118*, 11026–11039.

(73) Park, M. H.; Choi, K.-W.; Choi, S.; Kim, S. K.; Choi, Y. S. Vibrational Structures of Methylamine Isotopomers in the Predissociative $\tilde{A}$ States: CH3NHD, CD3NH2, CD3NHD, and CD3ND2. *J. Chem. Phys.* **2006**, *125*, 084311.

(74) Ahn, D.-S.; Lee, J.; Choi, J.-M.; Lee, K.-S.; Baek, S. J.; Lee, K.; Baeck, K.-K.; Kim, S. K. State-Selective Predissociation Dynamics of Methylamines: The Vibronic and H/D Effects on the Conical Intersection Dynamics. *J. Chem. Phys.* **2008**, *128*, 224305.

(75) Levi, C.; Kosloff, R.; Zeiri, Y.; Bar, I. Time-Dependent Quantum Wave-Packet Description of H and D Atom Tunneling in N–H and N–D Photodissociation of Methylamine and Methylamine-D2. *J. Chem. Phys.* **2009**, *131*, 064302.

(76) Marom, R.; Levi, C.; Weiss, T.; Rosenwaks, S.; Zeiri, Y.; Kosloff, R.; Bar, I. Quantum Tunneling of Hydrogen Atom in Dissociation of Photoexcited Methylamine. *J. Phys. Chem. A* **2010**, *114*, 9623–9627.

(77) Ahn, D.-S.; Lee, J.; Choon Park, Y.; Sup Lee, Y.; Kyu Kim, S. Nuclear Motion Captured by the Slow Electron Velocity Imaging Technique in the Tunnelling Predissociation of the S1 Methylamine. *J. Chem. Phys.* **2012**, *136*, 024306.

(78) Thomas, J. O.; Lower, K. E.; Murray, C. Observation of NH X3Σ– as a Primary Product of Methylamine Photodissociation: Evidence of Roaming-Mediated Intersystem Crossing? *J. Phys. Chem. Lett.* **2012**, *3*, 1341–1345.

(79) Xiao, H.; Maeda, S.; Morokuma, K. Theoretical Study on the Photodissociation of Methylamine Involving S1, T1, and S0 States. *J. Phys. Chem. A* **2013**, *117*, 5757–5764.

(80) Epshtein, M.; Yifrach, Y.; Portnov, A.; Bar, I. Control of Nonadiabatic Passage through a Conical Intersection by a Dynamic Resonance. *J. Phys. Chem. Lett.* **2016**, *7*, 1717–1724.

(81) Zhou, C.; Gagliardi, L.; Truhlar, D. G. State-Interaction Pair Density Functional Theory for Locally Avoided Crossings of Potential Energy Surfaces in Methylamine. *Phys. Chem. Chem. Phys.* **2019**, *21*, 13486–13493.

(82) Parker, K. A.; Truhlar, D. G. Semiglobal Diabatic Potential Energy Matrix for the N–H Photodissociation of Methylamine. *J. Chem. Phys.* **2020**, *152*, 244309.

(83) Sobolewski, A. L.; Domcke, W.; Dedonder-Lardeux, C.; Jouvet, C. Excited-State Hydrogen Detachment and Hydrogen Transfer Driven by Repulsive $1\pi\sigma^*$ States: A New Paradigm for Nonradiative Decay in Aromatic Biomolecules. *Phys. Chem. Chem. Phys.* **2002**, *4*, 1093–1100.

(84) Ashfold, M. N. R.; Cronin, B.; Devine, A. L.; Dixon, R. N.; Nix, M. G. D. The Role of $\Pi\sigma^*$ Excited States in the Photodissociation of Heteroaromatic Molecules. *Science* **2006**, *312*, 1637–1640.

(85) Devine, A. L.; Nix, M. G. D.; Dixon, R. N.; Ashfold, M. N. R. Near-Ultraviolet Photodissociation of Thiophenol. *J. Phys. Chem. A* **2008**, *112*, 9563–9574.

(86) Ashfold, M. N. R.; Devine, A. L.; Dixon, R. N.; King, G. A.; Nix, M. G. D.; Oliver, T. A. A. Exploring Nuclear Motion through Conical Intersections in the UV Photodissociation of Phenols and Thiophenol. *Proc. Natl. Acad. Sci.* **2008**, *105*, 12701–12706.

(87) Lim, J. S.; Choi, H.; Lim, I. S.; Park, S. B.; Lee, Y. S.; Kim, S. K. Photodissociation Dynamics of Thiophenol-D1: The Nature of Excited Electronic States along the S-D Bond Dissociation Coordinate. *J. Phys. Chem. A* **2009**, *113*, 10410–10416.

(88) Xu, X.; Yang, K. R.; Truhlar, D. G. Diabatic Molecular Orbitals, Potential Energies, and Potential Energy Surface Couplings by the 4-Fold Way for Photodissociation of Phenol. *J. Chem. Theory Comput.* **2013**, *9*, 3612–3625.

(89) Zhu, X.; Malbon, C. L.; Yarkony, D. R. An Improved Quasi-Diabatic Representation of the 1, 2, 31A Coupled Adiabatic Potential Energy Surfaces of Phenol in the Full 33 Internal Coordinates. *J. Chem. Phys.* **2016**, *144*, 124312.

(90) Zhang, L.; Truhlar, D. G.; Sun, S. Electronic Spectrum and Characterization of Diabatic Potential Energy Surfaces for Thiophenol. *Phys. Chem. Chem. Phys.* **2018**, *20*, 28144–28154.

(91) Zhang, L.; Truhlar, D. G.; Sun, S. Full-Dimensional Three-State Potential Energy Surfaces and State Couplings for Photodissociation of Thiophenol. *J. Chem. Phys.* **2019**, *151*, 154306.

(92) Tseng, C.-M.; Lee, Y. T.; Ni, C.-K. H Atom Elimination from the $\Pi\sigma^*$ State in the Photodissociation of Phenol. *J. Chem. Phys.* **2004**, *121*, 2459–2461.

(93) Tseng, C.-M.; Lee, Y. T.; Lin, M.-F.; Ni, C.-K.; Liu, S.-Y.; Lee, Y.-P.; Xu, Z. F.; Lin, M. C. Photodissociation Dynamics of Phenol. *J. Phys. Chem. A* **2007**, *111*, 9463–9470.

(94) Hause, M. L.; Heidi Yoon, Y.; Case, A. S.; Crim, F. F. Dynamics at Conical Intersections: The Influence of O–H Stretching Vibrations on the Photodissociation of Phenol. *J. Chem. Phys.* **2008**, *128*, 104307.

(95) Dixon, R. N.; Oliver, T. A. A.; Ashfold, M. N. R. Tunnelling under a Conical Intersection: Application to the Product Vibrational State Distributions in the UV Photodissociation of Phenols. *J. Chem. Phys.* **2011**, *134*, 194303.

(96) Xu, X.; Zheng, J.; Yang, K. R.; Truhlar, D. G. Photodissociation Dynamics of Phenol: Multistate Trajectory Simulations Including Tunneling. *J. Am. Chem. Soc.* **2014**, *136*, 16378–16386.

(97) Xie, C.; Ma, J.; Zhu, X.; Yarkony, D. R.; Xie, D.; Guo, H. Nonadiabatic Tunneling in Photodissociation of Phenol. *J. Am. Chem. Soc.* **2016**, *138*, 7828–7831.

(98) Vieuxmaire, O. P. J.; Lan, Z.; Sobolewski, A. L.; Domcke, W. Ab Initio Characterization of the Conical Intersections Involved in the Photochemistry of Phenol. *J. Chem. Phys.* **2008**, *129*, 224307.

(99) Pastore, M.; Helal, W.; Evangelisti, S.; Leininger, T.; Malrieu, J.-P.; Maynau, D.; Angeli, C.; Cimiraglia, R. Can the Second Order Multireference Perturbation Theory Be Considered a Reliable Tool to Study Mixed-Valence Compounds? *J. Chem. Phys.* **2008**, *128*, 174102.

(100) Pastore, M.; Helal, W.; Angeli, C.; Evangelisti, S.; Leininger, T.; Cimiraglia, R. Application of a "Charge-Averaged" Second Order Multireference Perturbation Theory Strategy to the Study of a Model Mixed-Valence Compound. *J. Mol. Struct.: THEOCHEM* **2009**, *896*, 12–17.

(101) Cui, Q.; Morokuma, K.; Stanton, J. F. Ab Initio MO Studies on the Photodissociation of C2H2 from the S1 (1Au) State. Non-adiabatic Effects and S-T Interaction. *Chem. Phys. Lett.* **1996**, *263*, 46–53.

(102) Ventura, E.; Dallos, M.; Lischka, H. The Valence-Excited States T1–T4 and S1–S2 of Acetylene: A High-Level MR-CISD and MR-AQCC Investigation of Stationary Points, Potential Energy Surfaces, and Surface Crossings. *J. Chem. Phys.* **2003**, *118*, 1702–1713.

(103) Caricato, M.; Trucks, G. W.; Frisch, M. J.; Wiberg, K. B. Electronic Transition Energies: A Study of the Performance of a Large Range of Single Reference Density Functional and Wave Function Methods on Valence and Rydberg States Compared to Experiment. *J. Chem. Theory Comput.* **2010**, *6*, 370–383.

(104) Weber, P.; Reimers, J. R. Ab Initio and Density Functional Calculations of the Energies of the Singlet and Triplet Valence Excited States of Pyrazine. *J. Phys. Chem. A* **1999**, *103*, 9821–9829.

(105) Walker, I. C.; Palmer, M. H. The Electronic States of the Azines. IV. Pyrazine, Studied by VUV Absorption, near-Threshold Electron Energy-Loss Spectroscopy and Ab Initio Multi-Reference Configuration Interaction Calculations. *Chem. Phys.* **1991**, *153*, 169–187.

(106) Walker, I. C.; Palmer, M. H.; Hopkirk, A. The Electronic States of the Azines. II. Pyridine, Studied by VUV Absorption, near-Threshold Electron Energy Loss Spectroscopy and Ab Initio Multi-Reference Configuration Interaction Calculations. *Chem. Phys.* **1990**, *141*, 365–378.

(107) Cai, Z.-L.; Reimers, J. R. The Low-Lying Excited States of Pyridine. *J. Phys. Chem. A* **2000**, *104*, 8389–8408.

(108) da Silva, F. F.; Almeida, D.; Martins, G.; R. Milosavljević, A.; P. Marinković, B.; V. Hoffmann, S.; J. Mason, N.; Nunes, Y.; Garcia, G.; Limão-Vieira, P. The Electronic States of Pyrimidine Studied by VUV Photoabsorption and Electron Energy-Loss Spectroscopy. *Phys. Chem. Chem. Phys.* **2010**, *12*, 6717–6731.

(109) Feller, D.; Peterson, K. A.; Davidson, E. R. A Systematic Approach to Vertically Excited States of Ethylene Using Configuration Interaction and Coupled Cluster Techniques. *J. Chem. Phys.* **2014**, *141*, 104302.

(110) Watson, M. A.; Chan, G. K.-L. Excited States of Butadiene to Chemical Accuracy: Reconciling Theory and Experiment. *J. Chem. Theory Comput.* **2012**, *8*, 4013–4018.

(111) Hiraya, A.; Shobatake, K. Direct Absorption Spectra of Jet-cooled Benzene in 130–260 Nm. *J. Chem. Phys.* **1991**, *94*, 7700–7706.

(112) Huebner, R. H.; Meilczarek, S. R.; Kuyatt, C. E. Electron Energy-Loss Spectroscopy of Naphthalene Vapor. *Chem. Phys. Lett.* **1972**, *16*, 464–469.

(113) Flicker, W. M.; Mosher, O. A.; Kuppermann, A. Electron Impact Investigation of Electronic Excitations in Furan, Thiophene, and Pyrrole. *J. Chem. Phys.* **1976**, *64*, 1315–1321.

(114) Leopold, D. G.; Pendley, R. D.; Roebber, J. L.; Hemley, R. J.; Vaida, V. Direct Absorption Spectroscopy of Jet-cooled Polyenes. II. The 1 1B+u←1 1A-g Transitions of Butadienes and Hexatrienes. *J. Chem. Phys.* **1984**, *81*, 4218–4229.

(115) Mota, R.; Parafita, R.; Giuliani, A.; Hubin-Franskin, M. J.; Lourenço, J. M. C.; Garcia, G.; Hoffmann, S. V.; Mason, N. J.; Ribeiro, P. A.; Raposo, M.; Limão-Vieira, P. Water VUV Electronic State Spectroscopy by Synchrotron Radiation. *Chem. Phys. Lett.* **2005**, *416*, 152–159.

(116) Druzhinin, S. I.; Mayer, P.; Stalke, D.; von Bülow, R.; Noltemeyer, M.; Zachariasse, K. A. Intramolecular Charge Transfer with 1-Tert-Butyl-6-cyano-1,2,3,4-Tetrahydroquinoline (NTC6) and Other Aminobenzonitriles. A Comparison of Experimental Vapor Phase Spectra and Crystal Structures with Calculations. *J. Am. Chem. Soc.* **2010**, *132*, 7730–7744.

(117) Stein, T.; Kronik, L.; Baer, R. Reliable Prediction of Charge Transfer Excitations in Molecular Complexes Using Time-Dependent Density Functional Theory. *J. Am. Chem. Soc.* **2009**, *131*, 2818–2820.

TOC Graphic

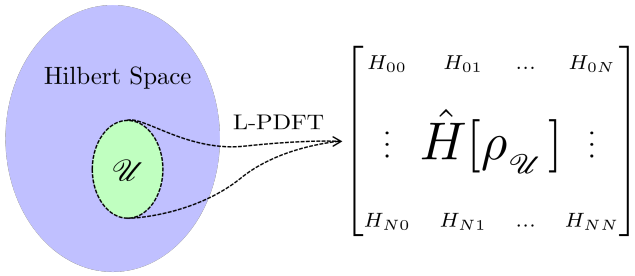
Hilbert Space
$\mathscr{U}$
L-PDFT
H_{00} H_{01} ... H_{0N}
$\hat{H}[\rho_{\mathscr{U}}]$
H_{N0} H_{N1} ... H_{NN}